# Diamagnetic shift of disorder-localized excitons in narrow GaAs/AlGaAs quantum wells

M. Erdmann,* C. Ropers, M. Wenderoth, and R. G. Ulbrich
*IV. Physikalisches Institut der Universität Göttingen, Friedrich-Hund-Platz 1, 37077 Göttingen, Germany*

S. Malzer and G. H. Döhler
*Max-Planck Research Group, Institute for Optics, Information, and Photonics, University of Erlangen-Nürnberg, Günther-Scharowsky-Strasse 1, 91058 Erlangen, Germany*

(Received 17 January 2006; revised manuscript received 9 June 2006; published 13 September 2006)

A correlation between the diamagnetic shift and transition energy of disorder-localized excitons is observed in magnetomicrophotoluminescence ($\mu$PL) on narrow GaAs/$Al_{0.3}Ga_{0.7}As$ quantum wells (QW's). The QW's were grown by molecular-beam epitaxy without growth interruption at the interfaces. $\mu$PL spectra were obtained in a confocal setup with the magnetic field applied normal to the QW plane. The lowest-energy exciton states have the smallest diamagnetic coefficients; the exciton diamagnetic shift in the localized exciton tail of the QW emission spectra increases by a factor of 2 as a function of transition energy. The positive correlation between diamagnetic shift and emission energy reveals exciton localization by short-range correlated interface disorder.

DOI: 10.1103/PhysRevB.74.125412 PACS number(s): 78.55.Cr, 78.67.−n, 78.20.Ls, 68.35.Ct

## I. INTRODUCTION

Interface roughness of narrow quantum wells (QW's) leads to the localization of excitons[1,2] and causes inhomogeneous broadening of spatially averaged QW exciton spectra. As an extended particle, the exciton is a probe of (lateral) confinement. Its Bohr radius defines a natural length scale ($a_B \approx 10$ nm in GaAs). With respect to exciton localization, three length scales of disorder can be distinguished: (i) statistical disorder on the atomic scale, (ii) disorder on the length scale of the exciton Bohr radius in the QW, and (iii) long-range disorder. In this paper, we focus on the influence of short-scale disorder — in the range between (i) and (ii) — on exciton localization; i.e., we study disorder localization near the *white noise* limit.[3] Figure 1 shows a simulated cross section of a GaAs/$Al_{0.3}Ga_{0.7}As$ QW with statistical distribution of Al atoms in the barriers and ideal, planar interfaces at distance $d$. In QW's grown without growth interruption, inhomogeneities in the distribution of Al atoms cause short-range interface disorder on a nm scale, leading to sizable fluctuations of the local band edges on the length scale of the exciton Bohr radius.

Localization of excitons in disordered narrow QW's is determined by the combination of the Coulomb interaction between electrons and holes and electron and hole confinement caused by fluctuations of the local band edges. For sufficiently thin wells, the model of a three-dimensional exciton moving between the corrugated QW interfaces is replaced by that of a quasi-two-dimensional exciton in a lateral disorder potential.[4] In QW's with short-range disorder in the interfaces, the exciton averages over the underlying disorder with its relative wave function (Fig. 2). Local minima in this effective disorder potential for the exciton center of mass (Fig. 2) act as natural quantum dots (QD's), also called quantum well dots (QWD's). The size and shape of the exciton wave function (WF) in QWD's are determined by parameters of the QW interface disorder. Optical methods with high spectral and spatial resolution ($<1$ $\mu$m) such as microphotoluminescence ($\mu$PL) or near-field optical microscopy enable the study of single-dot properties of individual localized exciton states—e.g., exciton diamagnetic shift (XDS).

Exciton diamagnetic shift has been studied experimentally for excitons in low-dimensional quantum structures (QW, QWR, QD) (Refs. 5–8) and for disorder-localized excitons in narrow QW's (Refs. 9–12). The XDS of exciton ground states is a measure of the extension of the relative wave function perpendicular to the magnetic field.[13–16] For disorder-localized excitons in narrow QW's, a variation of the XDS between different exciton eigenstates has been observed.[9] Besides the exciton radius, the exciton in-plane

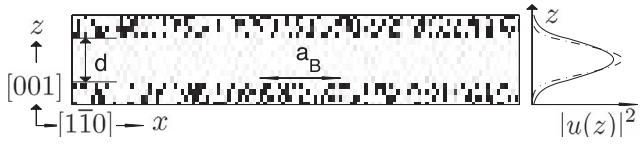


FIG. 1. Simulated cross section of a 4-nm GaAs/$Al_{0.3}Ga_{0.7}As$ QW with perfect interfaces and statistically distributed Al atoms in the barriers (marked in black). Lateral exciton Bohr radius $a_B$ and probability densities $|u(z)|^2$ of $z$ wave functions for electrons (solid line) and holes (dash-dotted) in a perfect QW heterostructure are shown.

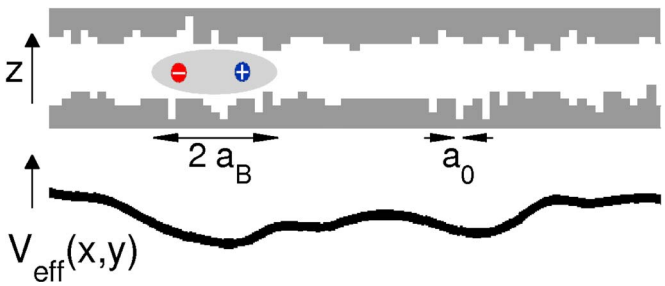


FIG. 2. (Color online) Schematic view of an exciton in a QW with rough interfaces and corresponding effective potential $V_{eff}$ for the exciton center of mass.

 

reduced mass influences the XDS. Consequently, a quantitative interpretation of the diamagnetic shift requires consideration of confinement-related mass enhancement effects in QW's.[13,17,18] Recent experiments showed a significant influence of conduction band nonparabolicity in narrow QW's on the exciton in-plane reduced mass.[19] This paper puts a focus on the effect of interface disorder in narrow QW's on the exciton diamagnetic shift, specifically on the relation between XDS and localization energy.

It presents experimental results of high-spatial-resolution magnetoluminescence spectroscopy on 2-nm and 4-nm $GaAs/Al_{0.3}Ga_{0.7}As$ QW's grown by molecular-beam epitaxy (MBE) without growth interruption at the interfaces. Luminescence spectra of the QW's show no monolayer (ML) splitting. At low excitation density and low temperature, the spectrally sharp emission lines of localized exciton states are observed in the low-energy tail of $\mu$PL spectra. We observe Zeeman splitting and XDS of individual exciton states with a $B$ field applied normal to the QW plane.

The paper is structured as follows: Section II covers the conceptual description of exciton disorder localization and the interpretation of the diamagnetic shift; in Sec. III the magnetoluminescence experiments are described; and in Sec. IV the experimental results for the XDS are presented. Section V contains a discussion of our experimental findings. The results are summarized in Sec. VI.

## II. CONCEPT

The theoretical description of exciton localization has been developed in the envelope function framework.[4,16] For narrow QW's with not too strong interface fluctuations, localization of excitons is properly described in terms of lateral localization of the exciton in-plane wave function. If confinement in the direction normal to the well (vertical or $z$ confinement) is strong compared to lateral confinement $(x,y)$, electronic subbands are well separated. Using the envelope function formalism, the motion of electron and hole in the $z$ direction can approximately be factored out from the full exciton wave function, separating $3d$ vectors into in-plane $(\boldsymbol{\rho_e},\boldsymbol{\rho_h})$ and $z$ components and taking only the lowest electron and hole subbands into account.[20] This separation ansatz leads to a factorization of the full wave function of an exciton state $\alpha$ in the lowest-subband electron and hole $z$ wave functions $u_e(z_e)$ and $u_h(z_h)$, respectively, and the in-plane exciton wave function $\phi_\alpha(\boldsymbol{\rho}_e,\boldsymbol{\rho}_h)$,

$$\Psi_\alpha(\boldsymbol{\rho}_e,\boldsymbol{\rho}_h,z_e,z_h) = u_e(z_e)u_h(z_h)\phi_\alpha(\boldsymbol{\rho}_e,\boldsymbol{\rho}_h). \tag{1}$$

The exciton in-plane motion in QW's with interface roughness is described by the two-particle Schrödinger equation, including Coulomb interaction and disorder potentials $V_e(\boldsymbol{\rho_e})$, $V_h(\boldsymbol{\rho_h})$ for electrons and holes, representing the spatial variation of the local band edges. The determination of $V_e(\boldsymbol{\rho_e})$ and $V_h(\boldsymbol{\rho_h})$ from underlying disorder in the QW interfaces has been described in detail in theoretical work.[4]

For the case of weak disorder—i.e., when disorder strength on the length scale of the exciton Bohr radius is smaller than exciton binding energy—a simplified model has been developed: This model assumes that disorder influences mainly exciton center-of-mass (c.m.) motion and that in-plane relative and c.m. motion can be separated.[4] To describe in-plane relative and c.m. motion, we define the total exciton mass $M=m_e+m_h$, the in-plane c.m. coordinate $\boldsymbol{R}=(m_e\boldsymbol{\rho}_e+m_h\boldsymbol{\rho}_h)/M$, the reduced mass $\mu=m_em_h/M$, and the in-plane relative coordinate $\boldsymbol{\rho}=\boldsymbol{\rho}_e-\boldsymbol{\rho}_h$. The two-particle WF $\phi$ is factorized into a product of a c.m. WF $\psi(\boldsymbol{R})$ and relative WF $\varphi(\boldsymbol{\rho})$. To describe the relative motion, a $1s$ wave function $\varphi_{1s}(\boldsymbol{\rho}) \propto \exp(-\rho/a_B)$ is used which is rigid throughout the structure. In this simple factorization approach, the exciton averages over underlying disorder with its relative WF. Figure 2 schematically shows a narrow, disordered QW and the effective potential $V_{\text{eff}}(\boldsymbol{R})$ for the exciton center of mass resulting from this averaging process.[4]

In general, disorder leads to a coupling of exciton c.m. and relative motion. Lateral confinement of the exciton center-of-mass reduces the exciton radius, so we describe the relative WF of localized exciton states by a $1s$ wave function with a Bohr radius $a_B$ smaller than that of a laterally free QW exciton. A magnetic field $B$ normal to the QW plane increases the transition energy of a given exciton state $\alpha$,

$$E_\alpha(B) = E_\alpha(B=0) + \Delta_\alpha(B). \tag{2}$$

Using first-order perturbation theory, the diamagnetic shift $\Delta_\alpha$ of a $1s$ exciton state $\alpha$ is expressed by[21]

$$\Delta_\alpha(B) = \frac{e^2}{8\mu}\langle\rho_\alpha^2\rangle B^2, \tag{3}$$

where $\langle\rho_\alpha^2\rangle^{1/2}$ is the effective lateral exciton radius. The expression for the XDS is more complicated in the presence of disorder.[16] Within the scope of the discussion of our experimental results, it is, however, reasonable to use Eq. (3) and to express the diamagnetic shift $\Delta_\alpha$ by the diamagnetic coefficient

$$\gamma_2^{(\alpha)} = \frac{e^2}{8\mu}\langle\rho_\alpha^2\rangle. \tag{4}$$

Confinement influences both the effective exciton radius $\rho_\alpha$ and the exciton reduced mass $\mu$ (Ref. 19): Stronger confinement decreases the exciton radius and increases the exciton reduced mass $\mu$. Both factors decrease the diamagnetic coefficient. Therefore, a reduction of the XDS is consistently interpreted as a confinement effect. Quantitative interpretation of XDS values requires consideration of the dependence of the in-plane electron mass and, consequently, the in-plane exciton reduced mass, on the QW width.

Experimentally, the diamagnetic shift of localized exciton levels is determined from the $B$-field-dependent optical spectra by taking the mean value of the Zeeman components. The magnetic length scale given by $\lambda=\sqrt{\hbar/eB}$ determines the crossover from the low-field to high-field regime. As long as $\lambda \ll a_B$ or, equivalently, if the cyclotron energy $\hbar eB/\mu$ is much smaller than the exciton binding energy $E_B$, the $B$ dependence of the exciton energy is dominated by a diamagnetic shift. For a perfect 4-nm $GaAs/Al_{0.3}Ga_{0.7}As$ QW, an exciton Bohr radius $a_B \approx 8.5$ nm is predicted using a variational method,[22] and therefore

$$\lambda(B = 8T) \approx a_B. \tag{5}$$

Therefore, the diamagnetic coefficient is determined by a quadratic fit of the mean value of the Zeeman components up to $B=4$ T. At higher fields, the cyclotron confinement of electrons and holes causes a deviation from the quadratic shift. In the high-field limit, the cyclotron energy $\hbar\omega_c$ dominates over the exciton Coulomb energy $E_B$ and a Landau-like linear increase of energy with magnetic field is predicted.[23] The $B$ dependence of the exciton diamagnetic shift for any magnetic field is therefore well described by an interpolation formula

$$\Delta(B) = a\frac{B^2}{\sqrt{b^2 + B^2}}. \tag{6}$$

The diamagnetic coefficient

$$\gamma_2 = \lim_{B\to 0} \frac{1}{2}\frac{d^2\Delta(B)}{dB^2} \tag{7}$$

is obtained from the fit as $\gamma_2 = a/b$. The parameters $a$ and $b$ are determined by fitting the mean value of the Zeeman components up to $B=10$ T. This fit procedure leads to nearly identical results for the diamagnetic coefficient $\gamma_2$ as the quadratic fit up to 4 T.

## III. EXPERIMENT

Two GaAs/$Al_{0.3}Ga_{0.7}As$ single QW samples ($QW_1$, $QW_2$) were grown by MBE on exactly (001) oriented, $n$-doped ($10^{18}$ $cm^{-3}$) GaAs substrates. A 50-nm-thick intrinsic GaAs buffer layer was grown directly on the substrate. In case of sample $QW_1$, intrinsic GaAs QW's with 4, 6, 8, 10, and 20 nm nominal thickness each surrounded by 15-nm-thick barriers of intrinsic $Al_{0.3}Ga_{0.7}As$ were grown on the buffer layer without growth interruption. In the case of sample $QW_2$, intrinsic GaAs QW's with 2, 4, 6, and 8 nm nominal thickness each surrounded by 20-nm-thick barriers of intrinsic $Al_{0.3}Ga_{0.7}As$ were grown. In both samples, a second 50-nm $i$-GaAs buffer layer and a 100-nm $n$-GaAs capping were grown on top of the QW heterostructures.

The sample structure was designed for the combined study of optical and structural properties of the QW's. At room temperature (RT), the carrier concentration in the QW increases by diffusion of carriers from the $n$-doped barriers into the wells. This enables imaging of QW cross sections by scanning tunneling microscopy (STM) at RT.[24] For the spectroscopic studies, the samples were mounted directly on the back face plate of a Cassegrain mirror objective. This objective was placed in the flow cryostat inset of a superconducting magnet. The $\mu$PL measurements were performed at 3 K. At this temperature, the carrier concentration in the wells from the doping in the spatially remote $n$-type layers is negligible. A magnetic field of up to 12 T could be applied normal to the QW planes (Faraday configuration). In the optical measurements, a spatial resolution of 500 nm [full width at half maximum (FWHM) of the measured point spread function] was obtained using a confocal setup. The PL was excited by a cw argon laser (514 nm, linearly polarized) with a power density of $\sim 10$ W/$cm^2$. The luminescence signal was dispersed with a 0.6-m monochromator and detected with a liquid-nitrogen-cooled charged-coupled device camera. The spectral resolution of the optical system was 150 $\mu$eV.

## IV. RESULTS

Magneto-$\mu$PL spectra of the 4-nm QW in sample $QW_1$ and the 2-nm QW in sample $QW_2$ were studied with the $B$ field applied in Faraday configuration. The luminescence intensity is mainly attributed to a recombination of heavy-hole excitons in the QW. Due to breaking of the crystal symmetry by the QW interfaces, light-hole and heavy-hole states are split in energy by several meV.[25] Emission of light-hole excitons can be safely neglected.[20] The heavy-hole exciton consists of an electron with spin $S_e = 1/2$, $S_{e,z} = \pm 1/2$ and a heavy hole with effective spin $J_h = 3/2$ and $J_{h,z} = \pm 3/2$. The heavy-hole exciton multiplet is split into doublets by the short-range part of the exchange interaction, independent of the symmetry of the exciton state.[26] The doublets are characterized by their angular momentum projections $M = S_{e,z} + J_{h,z}$. The doublet with $|M| = 1$ is optically active (bright), while the doublet with $|M| = 2$ is optically inactive (dark) and therefore not observed in the emission spectra.

Low-temperature $\mu$PL spectra of the QW's were obtained during linearly polarized optical excitation with $\sim 10$ W/$cm^2$ at 514 nm. In Fig. 3(a), $\mu$PL spectra of the 2-nm GaAs/$Al_{0.3}Ga_{0.7}As$ QW at $B=0$ T and $B=10$ T are shown. The $\mu$PL spectra consist of sharp lines on top of a broad background. The spectrally sharp emission lines can be attributed to recombination of localized excitons. Emission from exciton states as low as 20 meV below the center of the QW emission peaks is observed. The homogeneous linewidth and zero-field exchange splitting[27] of the emission lines are not resolved due to the instrumental resolution of 150 $\mu$eV.

The emission spectra at zero magnetic field [Figs. 3(a) and 4(a)] show approximately Gaussian inhomogeneous broadening. The FWHM of the emission spectra are $\Gamma_0 = 4.5$ meV for the 4-nm QW and $\Gamma_0 = 7$ meV for the 2-nm QW. Effective disorder strengths on the length scale of the exciton Bohr radius in the QW can be determined from the FWHM of QW absorption spectra, which is typically larger than the FWHM of luminescence spectra.[4] Inhomogeneous broadening of absorption spectra has been estimated,[28] and an effective disorder strength $\sigma \approx 0.3$ ML on the length scale of the exciton Bohr radius has been obtained for both QW's,[30] using the relation between disorder strength $\sigma$ and FWHM of a Gaussian distribution, $\mathrm{FWHM} = 2\sqrt{2\ln(2)}\sigma$. The QW exciton spectra show no ML splitting.

An external magnetic field causes Zeeman splitting of electron and hole levels in doublets with energy separation $\Delta E_e = g_e^* \mu_B B$ and $\Delta E_h = g_h^* \mu_B B$,[26] where $g_e^*$ and $g_h^*$ are effective $g$ factors for electrons and holes and $\mu_B = e\hbar/2m_0 = 57.9$ $\mu$eV/T is the Bohr magneton. Depending on the geometric confinement, the effective $g$ factors may considerably differ from bulk values, which are determined by Luttinger parameters. The linear Zeeman splitting of localized exciton states is described by an exciton $g$ factor $g_{ex}^* = g_e^* + g_h^*$.[32]

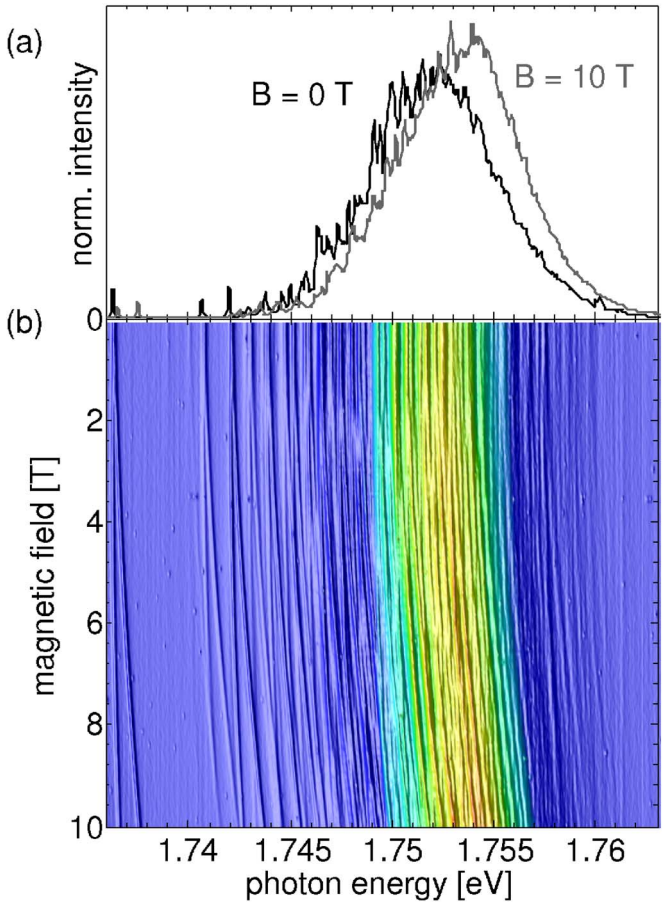


FIG. 3. (Color online) (a) $\mu$PL spectra of the 2-nm $GaAs/Al_{0.3}Ga_{0.7}As$ QW at $B=0$ T (black) and $B=10$ T (gray). (b) Magneto-$\mu$PL spectrum ($B=0-10$ T) of the 2-nm $GaAs/Al_{0.3}Ga_{0.7}As$ QW. The magnetic field was increased in steps of 50 mT.

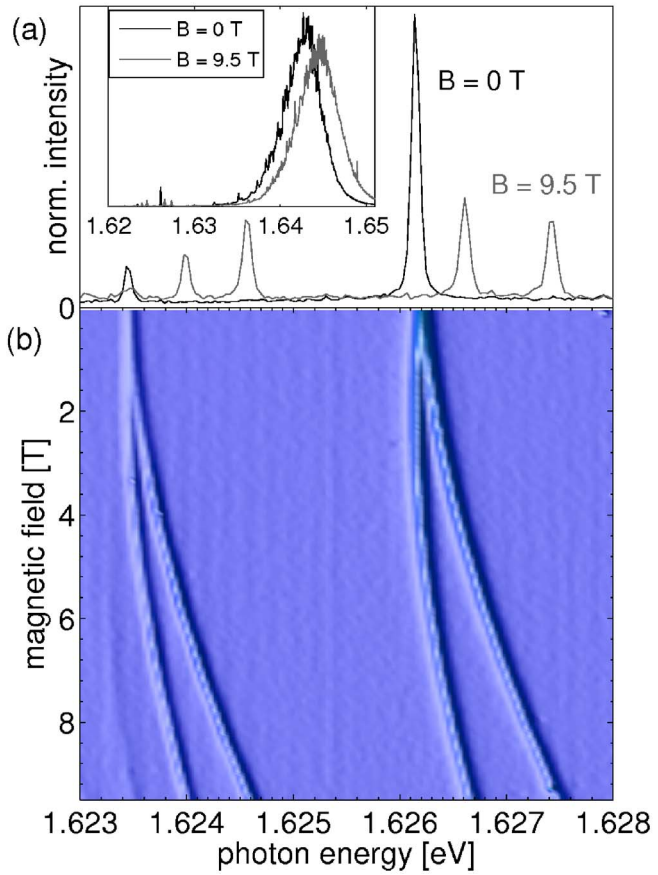


FIG. 4. (Color online) (a) Inset: $\mu$PL spectra of the 4-nm $GaAs/Al_{0.3}Ga_{0.7}As$ QW at $B=0$ T and $B=9.5$ T; emission lines of two localized exciton states at $B=0$ T (black) and $B=9.5$ T (gray). (b) Magneto-$\mu$PL spectrum ($B=0-9.5$ T) showing Zeeman splitting and diamagnetic shift of two of the lowest-energy localized exciton states in the 4-nm QW.

In Fig. 3(b), color-coded $\mu$PL spectra of the 2-nm QW are shown for magnetic fields between $B=0$ T and $B=10$ T. Zeeman splitting of the localized exciton states is resolved above $B=1$ T. The Zeeman components of the lowest-energy exciton states are clearly identified in Figs. 3 and 4. Higher-lying lines are less well separated, and for several closely spaced states at the QW emission peak it is impossible to trace the Zeeman components over the complete $B$-field range. However, for several emission lines unambiguous identification is possible. As an example, Fig. 5 shows two higher-lying emission lines below the QW emission peak of the 2-nm QW.

Figure 6 shows diamagnetic coefficients of localized exciton states in the 2-nm and 4-nm $GaAs/Al_{0.3}Ga_{0.7}As$ QW's as a function of transition energy. The top energy axis is the common energy axis for both QW's; zero energy is chosen as the center of a simulated QW absorption spectrum.[33] The determination of diamagnetic coefficients from $\mu$-magnetoluminescence spectra has been described in Sec. II. The diamagnetic coefficients at the emission peaks of both QW's are shown as solid symbols. The emission peak of the 4-nm QW shifts with $\gamma_2=22$ $\mu eV/T^2$, while for the emission peak of the 2-nm QW, a diamagnetic coefficient $\gamma_2$

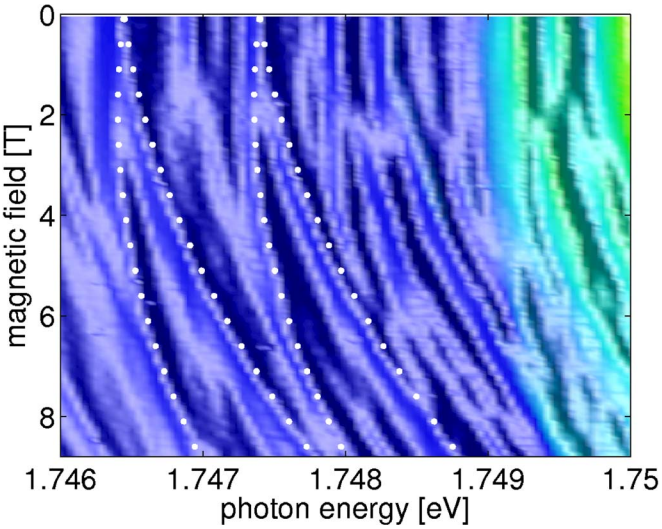


FIG. 5. (Color online) Section of Fig. 3(b): The dotted lines mark Zeeman components of two higher-energy emission lines below the 2-nm QW emission peak.

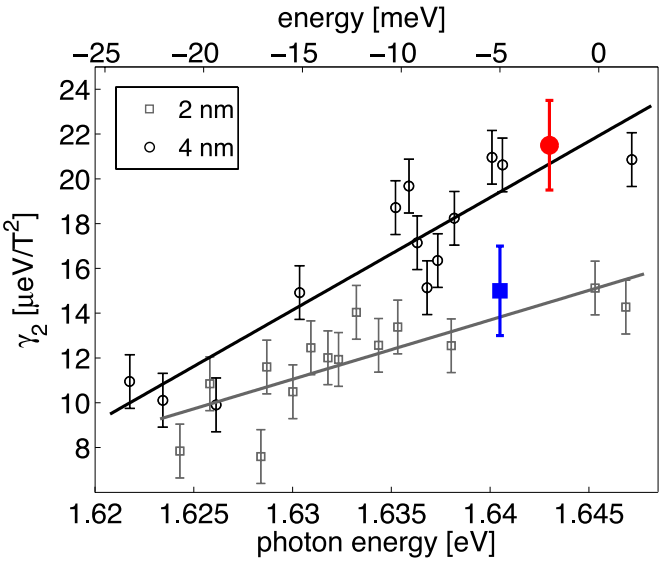


FIG. 6. (Color online) Diamagnetic coefficients of exciton states in 2-nm (gray squares) and 4-nm (black circles) $GaAs/Al_{0.3}Ga_{0.7}As$ QW's as a function of transition energy. The bottom energy axis applies to the 4-nm QW; values for the 2-nm QW have been shifted by −110 meV. Zero of the top energy axis is the center of a simulated QW absorption spectrum—i.e., QW emission peak energy plus Stokes shift (2-nm QW: 5 meV, 4-nm QW: 2.5 meV). Diamagnetic coefficients at the QW emission peaks are shown as solid symbols.

$=15\ \mu eV/T^2$ is observed. The lowest-energy exciton states are observed ~20 meV below the QW emission peaks. The lowest exciton states in the 4-nm QW have diamagnetic coefficients of $\sim 10\ \mu eV/T^2$, less than 1/2 the magnitude of the XDS at the QW emission peak. For the 2-nm QW, the diamagnetic coefficients of the lowest exciton states are reduced to $\sim 8\ \mu eV/T^2$. The diamagnetic coefficients show a systematic increase with transition energy. The slope of the trend line the for the 2-nm QW is smaller than that for the 4-nm QW. The qualitative statement that a positive correlation between XDS and localization energy of localized exciton states exists in our QW samples is the central result of our work.

## V. DISCUSSION

This section discusses the experimental results for the diamagnetic shift of localized excitons in the narrow $GaAs/Al_{0.3}Ga_{0.7}As$ QW's, and the interpretation of the observed correlation between XDS and localization energy in terms of the QW interface structure.

Confinement-dependent reduction of diamagnetic coefficients has been observed for excitons in quantum structures—i.e., QW, QWR, and QD.[5,7,8] The confinement increases the overlap between electron and hole WF's, leading to a larger exciton binding energy and in turn to a smaller exciton Bohr radius. Consequently, the diamagnetic coefficient is a measure of confinement in these simple cases of nearly ideal 1*d*, 2*d*, or 3*d* confinement. The effect of QW confinement is apparent in Fig. 6: The average diamagnetic

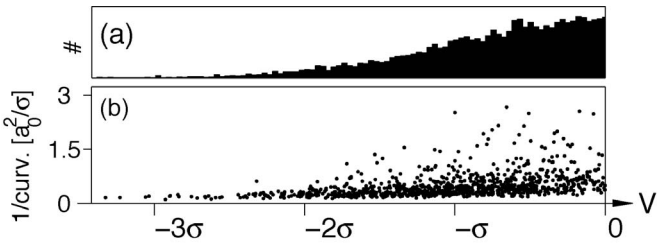


FIG. 7. (a) Histogram of a Gaussian disorder potential $V(r)$ with variance $\sigma^2$ and (b) inverse curvature of potential minima of the uncorrelated potential $V(r)$ as a function of potential values. $a_0$ denotes the lattice constant and # the number of potential values.

coefficient is larger for the 4-nm QW than for the 2-nm QW.

Exciton localization by random fluctuations of the local band edges in narrow QW's has been studied in recent theoretical work, taking the full Coulomb-correlated two-particle motion into account.[16] Energies and wave functions of exciton tail states were calculated with and without a *B* field normal to the QW plane, and diamagnetic shifts were determined from simulated optical spectra. A correlation between XDS and lateral WF extension was observed, showing that the most strongly localized exciton states have the smallest diamagnetic coefficients. This means that the XDS is a measure of lateral confinement also in the case of disorder-localized excitons.

In our experiments on 2-nm and 4-nm $GaAs/Al_{0.3}Ga_{0.7}As$ QW's, diamagnetic coefficients on the order of $10-20\ \mu eV/T^2$ have been observed for all localized exciton states (Fig. 6), showing that all observed exciton states are 1*s* states. An XDS more than one order of magnitude larger than for 1*s* excitons would be expected for 2*s* excitons because of their much larger lateral radius. Equation (4) and 2*s* wave functions for two-dimensional excitons[35] were used for this rough estimate. At the low excitation densities used in our experiments, biexcitons are not observed. We also have not found exceptionally small XDS on the order of 1 $\mu eV/T^2$, as reported by Phillips and co-workers for particular exciton states in a narrow $GaAs/Al_{0.3}Ga_{0.7}As$ QW.[11,12]

The positive slope observed in the XDS distribution as a function of transition energy (Fig. 6) shows that the lowest exciton tail states have the smallest diamagnetic coefficients, corresponding to small relative wave functions.[16] Consequently, the lowest exciton states are laterally strongly confined states. This result requires detailed discussion.

To explain the positive slope in Fig. 6, we consider the simple model of a one-dimensional uncorrelated, Gaussian distributed disorder potential $V(r)$ with variance $\sigma^2$ ("white noise"). Figure 7(a) shows a histogram of the potential values of $V(r)$ and Fig. 7(b) the inverse curvature of potential minima as a function of potential values. The inverse curvature is determined numerically from the discrete second derivative of $V(r)$ at the potential minima. The inverse curvature is a rough measure of lateral extension of potential minima. The result [Fig. 7(b)] shows a general property of random Gaussian disorder: The inverse curvature of potential minima increases with increasing potential values, which means deep potential minima are spatially narrow. This is plausible because the probability of finding several nearly

equal potential values $E$ on $L$ neighboring sites decreases with larger potential fluctuation $E$. The stated result can also be obtained in the framework of optimum fluctuation theory or with methods of statistical topography.[20,36]

To relate this feature of a random Gaussian-distributed disorder potential to exciton localization by this potential, it is necessary to take the averaging of the exciton over underlying disorder into account. We assume that the two-dimensional uncorrelated Gaussian potential $V(r)$ describes the spatial variation of the local band edges in the QW plane. The averaging with the exciton relative WF leads to a reduction of disorder strength and introduces correlations on the length scale of the exciton Bohr radius. Potential minima of the underlying disorder potential are smeared out. Taking the inverse curvature of potential minima as a measure for their lateral extension, we state that minima in the resulting effective potential $V_{\mathrm{eff}}(R)$ for the exciton center of mass extend over several minima of $V(r)$ (see Fig. 2), denoting with $R$ the c.m. coordinate of the exciton. Excitons are localized at positions where the underlying potential $V(r)$ is strongly reduced at several neighboring sites—i.e., where several deep minima of the uncorrelated disorder potential occur in close vicinity. The width and depth of minima in $V_{\mathrm{eff}}(R)$ are therefore determined by the probability of finding several deep minima in $V(r)$ at nearby sites. If $V(r)$ is uncorrelated or exhibits only short-range correlations below the length scale of the exciton Bohr radius, this probability decreases with increasing depth and number of potential minima involved. It is therefore plausible that deep minima of $V_{\mathrm{eff}}(R)$ tend to be spatially narrow.

It is important to note that the exciton radius is itself confinement dependent: Stronger lateral confinement leads to a reduced Bohr radius. Therefore, minima of the underlying disorder potential are not just averaged out with the same relative wave function; rather, the deep, narrow minima are averaged with the smallest WF's. Because averaging with a smaller relative WF is less effective, the inverse curvature of deep minima increases less than that of higher minima.

Figure 8 schematically shows several minima in the effective potential $V_{\mathrm{eff}}(R)$ for the exciton center of mass resulting from underlying short-range disorder, as well as transition energies and c.m. wave functions of local exciton ground states. Exciton states are schematically assigned to transitions in the low-energy tail of the $\mu$PL spectrum of a disordered QW. The total localization energy of an exciton state is inversely related to its localization volume. Short-scale well width fluctuations present near the *white noise* limit eventually lead to a strong local reduction of vertical confinement energy, resulting in deep, rare minima in $V_{\mathrm{eff}}(R)$. Our result that the lowest exciton states have the smallest diamagnetic coefficients (Fig. 6) means that exciton states in deep minima have small wave functions. This is schematically depicted in Fig. 8. The reduction in vertical confinement energy prevails over the increase in lateral confinement energy.

Recent theoretical work supports our explanation of the positive slope in Fig. 6 as a result of exciton localization by short-range correlated disorder.[16] In a theoretical study, a positive correlation between XDS and transition energy of exciton states localized by a random Gaussian potential was

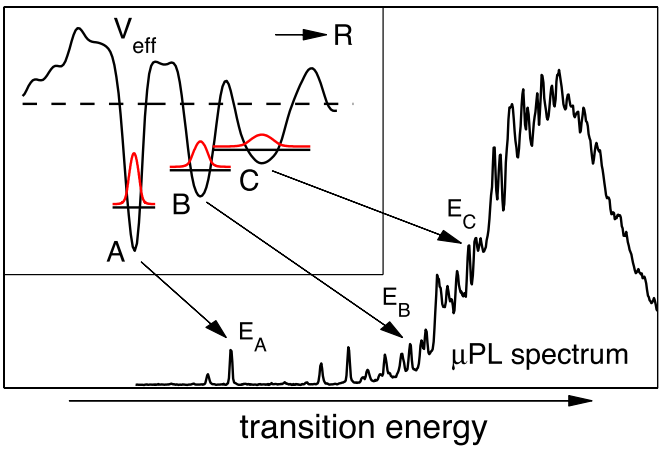


FIG. 8. (Color online) Schematic representation of the physical situation of exciton localization by short-range correlated disorder (inset). The effective potential $V_{\mathrm{eff}}(R)$ for the exciton center of mass and c.m. wave functions of exciton states in three potential minima $(A,B,C)$ are depicted. Exciton states are schematically assigned to transitions in the low-energy tail of the $\mu$PL spectrum of a disordered QW. Our experiment shows (Fig. 6) that deep-lying exciton states have small wave functions, as demonstrated in the inset.

observed. The lowest exciton states had diamagnetic coefficients of $\sim 10\ \mu\mathrm{eV/T}^2$. The XDS showed an increase by a factor of 3 over the range of the localized exciton tail of $\sim 20$ meV, in reasonable agreement with our experimental result. The positive correlation between XDS and transition energy enables the experimental study of exciton WF statistics. For random disorder it was shown that the XDS is determined by the local potential only. Consequently, study of exciton WF statistics allows the discrimination between several underlying disorder configurations.

We therefore relate the experimentally observed increase of the XDS as a function of emission energy to the interface structure of our samples. The qualitative agreement between our experimental result (Fig. 6) and theoretical XDS calculations for exciton localization by random Gaussian disorder,[16] which both show an increase of the XDS as a function of transition energy, reveals that lateral confinement of the exciton states in our samples is caused by short-range interface disorder. Indeed, large-scale (160-nm) cross-sectional STM topography of the 4-nm $\mathrm{GaAs/Al_{0.3}Ga_{0.7}As}$ QW obtained in a recent study shows mainly short-range correlations on the atomic scale.[24]

To demonstrate that exciton WF statistics provides information about interface disorder, we consider a different scenario of exciton localization, where a negative slope is expected for the relation between the XDS and localization energy. We focus on localization of excitons by ML islands in the interfaces of a QW. This type of disorder has been found for $\mathrm{GaAs/Al_{0.3}Ga_{0.7}As}$ QW's grown with growth interruption.[37] For islands with diameters on the order of the exciton Bohr radius, the diamagnetic shift of a localized exciton state will be proportional to the area of the island, while the lateral confinement energy is inversely proportional to that area. The vertical confinement energy is independent of the lateral extension of an island. Therefore, there

is a different relation between lateral extension of fluctuations and transition energy of localized exciton states than in the previously studied case of short-range disorder: The lowest exciton states will show the largest diamagnetic shift. As a result, negative slope in the XDS distribution of localized exciton states as a function of transition energy (Fig. 6) would be expected if only ML fluctuations were present in the QW interfaces.[38] The positive slope observed in our experiment therefore excludes this situation. Also note that we observe no ML splitting in the QW luminescence spectra. The energy difference corresponding to a ML fluctuation in the 2-nm QW is ~20 meV.[30]

Finally, we compare our experimental diamagnetic coefficients with theoretical results. For laterally free excitons in a 4-nm $GaAs/Al_{0.3}Ga_{0.7}As$ QW (corresponding to $E=0$ in Fig. 6), theoretical calculations obtained a diamagnetic coefficient $\gamma_2=44\ \mu eV/T^2$, assuming bulk values for the electron in-plane mass.[15,16] However, our experimental diamagnetic coefficient of $\sim 22\ \mu eV/T^2$ observed for the emission peak of the 4-nm QW is consistent with previous experimental studies: In all magnetoluminescence experiments of ~5-nm-wide $GaAs/Al_{0.3}Ga_{0.7}As$ QW's, values of $\sim 25\ \mu eV/T^2$ have been found.[5–7] Previous studies attributed discrepancies between experimental and theoretical values for QW diamagnetic coefficients to exciton localization[39] or to confinement-related enhancement of the exciton in-plane reduced mass.[13] Since we observe the strongest reduction of the XDS for the lowest-energy exciton states several meV below the QW emission peak, exciton localization is unlikely to explain the entire difference between our experimental XDS value at the QW emission peak and theoretical values for laterally free excitons. Rather, we attribute the discrepancy to the fact that the theoretical studies did not take the enhancement of the in-plane electron mass in narrow QW's into account. Newest calculations show that including the mass enhancement improves the agreement between our experiment and theory.[40]

## VI. CONCLUSIONS

We experimentally investigate the wave function statistics of disorder-localized excitons in narrow $GaAs/Al_{0.3}Ga_{0.7}As$ QW's using magneto-$\mu$PL spectroscopy. We determine diamagnetic coefficients of localized exciton states and observe positive slope in the distribution of diamagnetic coefficients as a function of transition energy in the localized exciton tail of the QW emission spectra. The positive slope in the relation between XDS and localization energy is a result of exciton localization by short-range correlated disorder. It is qualitatively consistent with results of theoretical work on the XDS of excitons localized by random Gaussian disorder in narrow QW's. The quantitative comparison of our experimental diamagnetic coefficients with theoretical results shows that the in-plane electron mass in the narrow QW's is enhanced over the bulk value.

## ACKNOWLEDGMENTS

We gratefully acknowledge helpful discussions with M. Grochol, F. Grosse, E. Runge, and R. Zimmermann. This work was supported by the Deutsche Forschungsgemeinschaft via SFB 602.

*Electronic address: erdmann@ph4.physik.uni-goettingen.de

[1] C. Weisbuch, R. C. Miller, R. Dingle, A. C. Gossard, and W. Wiegmann, Solid State Commun. **37**, 219 (1981).
[2] A. Zrenner, L. V. Butov, M. Hagn, G. Abstreiter, G. Böhm, and G. Weimann, Phys. Rev. Lett. **72**, 3382 (1994).
[3] V. Savona, S. Haacke, and B. Deveaud, Phys. Rev. Lett. **84**, 183 (2000).
[4] R. Zimmermann, F. Grosse, and E. Runge, Pure Appl. Chem. **69**, 1179 (1997).
[5] S. Tarucha, H. Okamoto, Y. Iwasa, and N. Miura, Solid State Commun. **52**, 815 (1984).
[6] D. C. Rogers, J. Singleton, R. J. Nicholas, C. T. Foxon, and K. Woodbridge, Phys. Rev. B **34**, 4002 (1986).
[7] T. Someya, H. Akiyama, and H. Sakaki, Phys. Rev. Lett. **74**, 3664 (1995).
[8] M. Bayer, S. N. Walck, T. L. Reinecke, and A. Forchel, Phys. Rev. B **57**, 6584 (1998).
[9] H. F. Hess, E. Betzig, T. D. Harris, L. N. Pfeiffer, and K. W. West, Science **273**, 1740 (1994).
[10] A. G. Steffan and R. T. Phillips, Phys. Status Solidi A **190**, 541 (2002).
[11] A. G. Steffan and R. T. Phillips, Physica E (Amsterdam) **17**, 15 (2003).
[12] R. T. Phillips, A. G. Steffan, S. R. Newton, T. L. Reinecke, and R. Kotlyar, Phys. Status Solidi B **238**, 601 (2003).
[13] K. J. Nash, M. S. Skolnick, P. A. Claxton, and J. S. Roberts, Phys. Rev. B **39**, 10943 (1989).
[14] V. Halonen, T. Chakraborty, and P. Pietiläinen, Phys. Rev. B **45**, 5980 (1992).
[15] S. N. Walck and T. L. Reinecke, Phys. Rev. B **57**, 9088 (1998).
[16] M. Grochol, F. Grosse, and R. Zimmermann, Phys. Rev. B **71**, 125339 (2005).
[17] U. Ekenberg, Phys. Rev. B **40**, 7714 (1989).
[18] M. Städele, K. Hess, T. Ruf, and M. Cardona, J. Appl. Phys. **91**, 9435 (2002).
[19] N. Schildermans, M. Hayne, V. V. Moshchalkov, A. Rastelli, and O. G. Schmidt, Phys. Rev. B **72**, 115312 (2006).
[20] E. Runge, Solid State Phys. **57**, 149 (2002).
[21] J. J. Hopfield and D. G. Thomas, Phys. Rev. **122**, 35 (1961).
[22] P. Harrison, *Quantum Wells, Wires and Dots: Theoretical and Computational Physics* (Wiley, New York, 1999).
[23] O. Akimoto and H. Hasegawa, J. Phys. Soc. Jpn. **22**, 181 (1967).
[24] C. Ropers, M. Wenderoth, L. Winking, T. C. G. Reusch, M. Erdmann, R. G. Ulbrich, S. Malzer, G. H. Döhler, M. Grochol, F. Grosse, and R. Zimmermann (unpublished).
[25] L. C. Andreani, A. Pasquarello, and F. Bassani, Phys. Rev. B **36**, 5887 (1987).
[26] E. L. Ivchenko and G. Pikus, *Superlattices and Other Hetero-*

*structures* (Springer, New York, 1995).
[27] D. Gammon, E. S. Snow, B. V. Shanabrook, D. S. Katzer, and D. Park, Phys. Rev. Lett. **76**, 3005 (1996).
[28] From the logarithmic slope of the exponential high-energy tail of the QW $\mu$PL spectra, effective temperatures $T_{\mathrm{eff}}$ for photoexcited electrons (e) and holes (h) have been determined that are higher than the lattice temperature. For 2-nm and 4-nm QW's, $T=22.5$ K and $T=18$ K are obtained, in agreement with values reported in the literature (Ref. 29). For the FWHM of extrapolated absorption (high-temperature) spectra, values of 9 meV (2-nm QW) and 6 meV (4-nm QW) were obtained.
[29] C. Colvard, D. Bimberg, K. Alavi, C. Maierhofer, and N. Nouri, Phys. Rev. B **39**, 3419 (1989).
[30] A one-dimensional square-well model has been used to calculate single-particle ground-state energies for a perfect QW. For the $GaAs/Al_{0.3}Ga_{0.7}As$ band offset, the values $\Delta_e+\Delta_h=436$ meV and $\Delta_e:\Delta_h=65:35$ were used (Ref. 31).
[31] S. Adachi, *GaAs and Related Materials* (World Scientific, Singapore, 1994).
[32] M. J. Snelling, E. Blackwood, C. J. McDonagh, R. T. Harley, and C. T. B. Foxon, Phys. Rev. B **45**, 3922 (1992).
[33] Carrier relaxation in the inhomogeneously broadened QW exciton band is responsible for a *T*-dependent Stokes shift that varies with disorder strength (Ref. 34). Therefore, the peak energy of the QW luminescence is not a well-suited reference energy. To overcome this problem, the top energy axis is renormalized by the Stokes shift. It is approximately determined by extrapolating low-temperature luminescence spectra to higher temperatures, assuming Boltzmann distributions for electrons and holes and using the effective charge carrier temperatures determined from the high-energy tails. Stokes shifts of 5 meV (2-nm QW) and 2.5 meV (4-nm QW) were obtained.
[34] M. Gurioli, A. Vinattieri, J. Martinez-Pastor, and M. Colocci, Phys. Rev. B **50**, 11817 (1994).
[35] H. Haug and S. W. Koch, *Quantum Theory of the Optical and Electronic Properties of Semiconductors* (World Scientific, Singapore, 2004).
[36] I. M. Lifshitz, S. A. Gredeskul, and L. A. Pastur, *Introduction to the Theory of Disordered Systems* (Wiley, New York, 1988).
[37] R. Grousson, V. Voliotis, N. Grandjean, J. Massies, M. Leroux, and C. Deparis, Phys. Rev. B **55**, 5253 (1997).
[38] Z. Barticevic, M. Pacheco, C. A. Duque, and L. E. Oliveira, Phys. Rev. B **68**, 073312 (2003).
[39] W. Ossau, B. Jäkel, and E. Bangert, in *High Magnetic Fields in Semiconductor Physics*, edited by G. Landwehr, Vol. 71 of Springer Series in Solid State Sciences (Springer Verlag, Berlin, 1987), p. 213.
[40] M. Grochol (private communication).